Characterization of poroelastic targets for P- and S-waves using linear and non-linear AVO methods

Steven Kim and Kris Innanen

ABSTRACT

AVO is one aspect of seismic analysis that is largely used in industry. In this report, an examination of amplitude modelling, as typically viewed from a surface seismic acquisition experiment, is performed. The basis of this work is driven primarily by the research of Russell, Gray, and Hampson and their $f - m - r$ equation which is a linear poroelastic AVO formulation that quantifies fluid in the target medium. We would like to extend that formulation by showing the method in which non-linear poroelastic AVO approximations are derived in terms of models using two different sets of model parameters. The first that will be shown is in terms of perturbation and the other is reflectivity. Their analytical expressions will be shown for 1st order (linear), 2nd order (non-linear), and 3rd order (non-linear). Once we have shown all six poroelastic approximations, we will display the results against a synthetic model to view the variations that occur between each approximation. We will also show the stability that each approximation holds in an exercise that tests various modelling parameters.

INTRODUCTION

There are many formulations on characterizing amplitude information in seismic data. If we choose a model for layered media that behaves perfectly elastic and assume a plane wave signature from the source, we may define contrasts across an interfaces in terms of velocities and densities namely V_P, V_S, and ρ. But it is not always the case that our Earth model will always behave in this way. We may see all sorts of effects such as anelasticity, viscolelasticity, or anisotropy that highly distort reflectivity information as it is being collected at the receiver. It may be permissible in certain circumstances where these effects are small enough to model the Earth where these wave altering effects may be averaged such that another Earth model may be reconstructed that reproduces the same amplitude response but is instead homogeneous, isotropic, and elastic. In other words, a simplification to a complex problem. This is possible if a-priori information can be extracted from either the seismic data or well logs. Even if information is known about the geology, a reconstruction of an Earth model that assumes these ideal properties still prove to be problematic as a direct inversion of the Zoeppritz equations is unstable (Russell et al., 2011).

In addition to anisotropy and other unfavourable effects, porosity and fluid-filled media also provide a challenge in interpreting seismic data but may be remedied through geophysical amplitude analysis. Interpreting these data depends on the criteria the geophysicist decides to use. The criteria being the level of porosity and fluid-filled content is available inside the geological target. From a modelling standpoint, there are infinite combinations of percentage porosity and differing fluid levels that the geophysicist can choose from however, it is with cautionary discretion that the geophysicist must consider. New methods are continuously being developed and tested that provide deeper insight. In the case of AVO in conjuction with Biot (1941) and Gassmann (1951) thoery, Russell et al.

(2011) has developed a linearized poroelastic AVO equation that is able to account for gas-filled pore space contributions. The goal of this report is to not only reproduce results that have been proposed by Russell et al. (2011) but to demonstrate another approach in regards to first (linear) and higher order poroelastic AVO and compare its behaviour with Russell and Gray's formulation. In the following sections: we will briefly describe poroelasticity and how it affects elastic media, show a convenient form of the Zoeppritz equations and how to incorporate poroelasticity theory within those equations, derive the first and second order poroelastic AVO equations, and present synthetic results.

POROELASTICITY

For elastic media, expressions for P- and S-wave velocities can be written such that

$$V_P^2 = \frac{\lambda + 2\mu}{\rho} = \frac{K + \frac{4}{3}\mu}{\rho} = \frac{s}{\rho}, \tag{1}$$

and

$$V_S^2 = \frac{\mu}{\rho}, \tag{2}$$

where λ is one of Lamé's constants, μ represents shear modulus (rigidity), K represents bulk modulus (incompressibility), ρ is density, and s is the "skeleton" term (Russell et al., 2011). As mentioned previously, Biot (1941) and Gassmann (1951) have developed a fluid compensation mechanism that can be applied directly to elastic constants. This type of compensation is also known as a Gassmann fluid substitution which is derived using stress-strain relationships and how these relationships affect acoustic properties that are fluid-filled. After making the substitution, a fluid modulus is placed inside of equation (1). Equation (2) does not include a fluid modulus because fluids have negligible effects on S-waves. The reasoning behind this will be shown below. An illustration that demonstrates why a Gassmann substitution may be necessary is shown in figure (1) which describes the pore/fluid system in a given rock sample (Russell et al., 2003). We will call this rock sample a sandstone for simplicity. With this sandstone, we may intuitively understand that replacing the pore spaces with the same material that make up the rock matrix would therefore produce a rock sample made entirely of the rock matrix. Thus, the sandstone would become entirely homogeneous. We may also describe the pore spaces of the sample to be "saturated" with sand. We will then use the term, saturated, as a more general way of expressing the following quantities. Although Biot-Gassmann theory does not account for substituting solid materials but for fluids, the idea is the same. The relations that describe fluid substitution are shown here where

$$\begin{aligned} \mu_{\text{sat}} &= \mu_{\text{dry}}, \\ \lambda_{\text{sat}} &= \lambda_{\text{dry}} + \alpha^2 M, \\ K_{\text{sat}} &= K_{\text{dry}} + \alpha^2 M, \end{aligned} \tag{3}$$

show the final result of deriving the poroelastic constants (Russell et al., 2011). These saturated constants describe the average distribution of fluid inside a rock sample. On the

right hand side of equation (3), the expression for $\alpha^2 M$ (fluid modulus) is also written in terms of elastic quantities

$$\alpha = 1 - \frac{K_{\text{dry}}}{K_{\text{m}}}, \tag{4}$$

and

$$\frac{1}{M} = \frac{\alpha - \phi}{K_{\text{m}}} + \frac{\phi}{K_{\text{fl}}}, \tag{5}$$

where K_{dry} is the skeletal bulk modulus, K_{m} is the matrix bulk modulus, ϕ represents the porosity, and K_{fl} is the bulk modulus of the fluid. The α term is regarded as the Biot coefficient which describes the linear relationship between x_{sat} and x_{dry} in equation (3). More specifically, in equation (4), the Biot coefficient will change depending on the bulk modulus ratio. This ratio will approach unity as the value for K_{dry} approaches K_{m}. This can be visualized in figure (1) where the entire rock sample will be made of the same material if $K_{\text{dry}} = K_{\text{m}}$ which implies that the dry modulus is the same as the saturated modulus in equation (3). Equation (5) also contributes to the linear relationship between x_{sat} and x_{dry} but contains more analytical complexity. Note that the fluid modulus does not contribute to the saturated shear modulus because fluids have little to no effect on shearing motions. Now that a better understanding between saturated and dry moduli has been established, we can substitute equation (3) into (1)-(2) to obtain poroelastic velocities which will be applied to the Zoeppritz equations. We write these poroelastic expressions for V_P and V_S such that

$$(V_P)^2_{\text{sat}} = \frac{\lambda_{\text{dry}} + 2\mu_{\text{sat}} + \alpha^2 M}{\rho_{\text{sat}}} = \frac{K_{\text{dry}} + \frac{4}{3}\mu_{\text{sat}} + \alpha^2 M}{\rho_{\text{sat}}}, \tag{6}$$

and

$$(V_S)^2_{\text{sat}} = \frac{\mu_{\text{sat}}}{\rho_{\text{sat}}}. \tag{7}$$

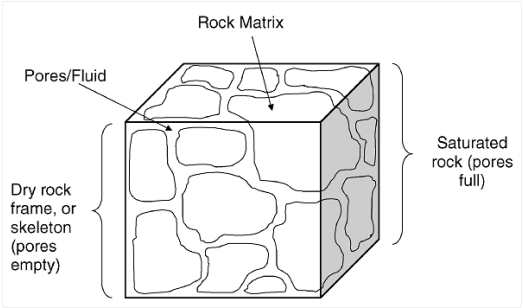

FIG. 1: This figure is adapted from Russell et al. (2003) which shows that a rock sample is composed of four components. These components include the dry rock (skeleton) frame, the saturated frame, the rock matrix, and pores/fluid (Russell et al., 2003). From this illustration, we can observe that there is a direct correlation between the dry frame and the saturated frame. This correlation being whether or not the pores are occupied by fluid.

REVIEW: ELASTIC ZOEPPRITZ EQUATIONS FOR INCIDENT P-WAVES

When a source is located on the surface of the Earth, it emits a wavefield that radially propagates through the subsurface. This is seen in figure (2) where a source has become active and is emitting a series of increasingly larger wavefronts that are propagating towards a boundary. For an elastic medium, the wavefronts are circular as there are no effects such as anisotropy that are disturbing the overall character of the wavefront. After a downgoing

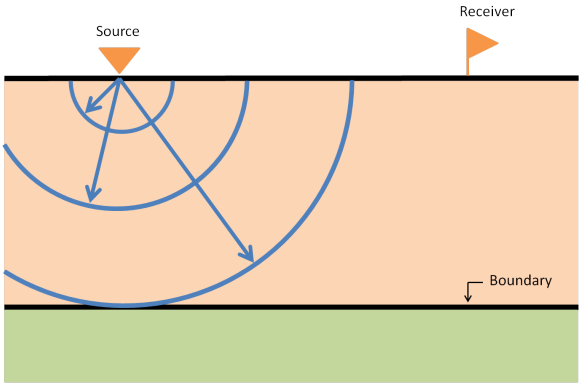

FIG. 2: A snapshot in time of a source that is emitting spherical wavefronts. Each wavefront can be described as an infinite series of straight rays where the tangent of said wavefront is perpendicular to a ray. Each arrow that is drawn from the source location represents one ray. Note that the wavefronts are circular for an elastic medium in 2D.

wavefront interacts with a boundary, a reflection and a transmission of that wavefront will occur. These two events are shown in figure (3) where some of the energy acting as upgoing wavefronts in the beige medium travels back towards the surface while the rest of the energy continues to travel down. Each circular wavefront in figures (2) and (3) is composed of an infinite series of straight rays where a few have been drawn for clarification in figure (2). These straight rays represent P-waves in this example. For each downgoing wavefront that interacts with the boundary there is an upgoing and transmitted wavefront associated, which accounts for three wavefronts total. The same principle applies for a P-wave ray. This is demonstrated in figure (4) where the aforementioned downgoing, upgoing, and transmitted P-waves are shown. Before the downgoing P-wave strikes the boundary, it must approach it at an angle. The angle θ is understood as the incidence angle that can be used as a measure of the other two P-wave angles using Snell's law to indicate direction. Although not shown in figures (2) and (3), S-wave wavefronts and S-wave rays behave in a similar manner to P-waves in a sense in which those angles are also calculated using Snell's law. Figure (4) merely shows the cause and effect of only P-waves in an elastic medium. However, mode conversion is analyzed in figure (5) where S-waves are produced. This is the reason for using the Zoeppritz equations. The Zoeppritz equations describe how these ray relationships hold based on conservation of reflection and transmission energy for both incidence P-waves and S-waves. For our study, we are mainly interested in the P-wave amplitude signature that the wavefield carries as it travels from the source; to a reflecting boundary; and to the receiver as seen in figure (4). Therefore, the Zoeppritz equations will be used to model these amplitudes. As mentioned previously, the incoming P-wave approaches the boundary at a particular angle θ. When $0^\circ < \theta < 90^\circ$, a reflected and transmitted P-wave is produced. Mode conversion also occurs where S-waves are generated from the incident P-wave. The direction and the amplitude of the reflected and transmitted

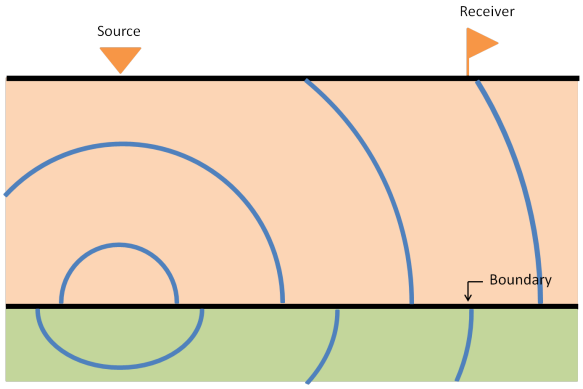

FIG. 3: A snapshot in time after the source has completed releasing energy and the remaining energy of the original wavefield is reflecting off of the boundary and is also being transmitted through the boundary. The energy that is reflected is recorded at the surface where the receiver is located while the transmitted energy continues to travel into the Earth.

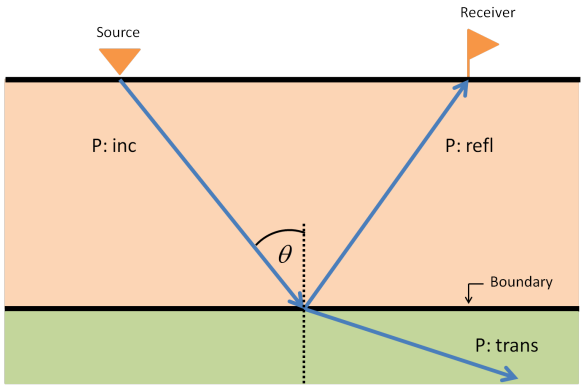

FIG. 4: This encaptures all paths that a P-wave may take which includes the incident, reflected, and transmitted wave. The dotted line refers to 90° from horizontal.

waves are based on two factors: the acoustic contrasts between medium 0 and medium 1 and the incident angle θ. These factors are explicitly shown in the Zoeppritz equations which quantify the behaviour of these P- and S-waves. In this section, we will observe

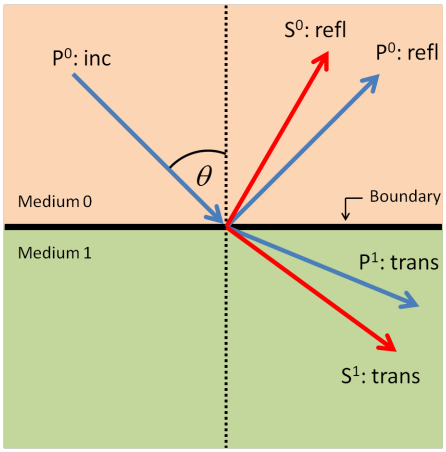

FIG. 5: A simplified model consisting of two homogeneous half-spaces separated by a welded contact. As the incident P-wave, P^0:inc, propagates toward the boundary at $\theta > 0$, a set of P- and S-waves will reflect off of the boundary and another set of P- and S-waves will transmit through the boundary into medium 1. The angle measured from normal for the two reflected and two transmitted waves all obey Snell's law.

one form of the Zoeppritz equations as shown by Keys (1989). It is a 4x4 matrix that shows geometric relationships of primary plane wave propagation and interface interaction using reflection and transmission coefficients. This relationship is more easily described in equation (8)

$$\begin{bmatrix} A_{11} & A_{12} & A_{13} & A_{14} \\ A_{21} & A_{22} & A_{23} & A_{24} \\ A_{31} & A_{32} & A_{33} & A_{34} \\ A_{41} & A_{42} & A_{43} & A_{44} \end{bmatrix} \begin{bmatrix} R_{\mathrm{PP}} \\ R_{\mathrm{PS}} \\ T_{\mathrm{PP}} \\ T_{\mathrm{PS}} \end{bmatrix} = \begin{bmatrix} b_1 \\ b_2 \\ b_3 \\ b_4 \end{bmatrix}, \tag{8}$$

where we can see linear combinations of these reflection and transmission coefficients. These are labeled as R_{ij} and T_{ij} respectively where i represents the initial wavefield and j represents the secondary wavefield. These linear combinations are proportional to the geometry of a geological setting as will be explained by the following. The elements of the first row of equation (8) are

$$A_{11} = -\sin\theta,$$

$$A_{12} = -\left[1 - \left(\frac{V_{S_0}^2}{V_{P_0}^2}\right)\sin^2\theta\right]^{1/2},$$

$$A_{13} = \left(\frac{V_{P_1}}{V_{P_0}}\right)\sin\theta,$$

$$A_{14} = -\left[1 - \left(\frac{V_{S_1}^2}{V_{P_0}^2}\right)\sin^2\theta\right]^{1/2},$$

the elements of the second row are

$$A_{21} = \left[1 - \sin^2\theta\right]^{1/2},$$

$$A_{22} = -\left(\frac{V_{S_0}}{V_{P_0}}\right)\sin\theta,$$

$$A_{23} = \left[1 - \left(\frac{V_{P_1}^2}{V_{P_0}^2}\right)\sin^2\theta\right]^{1/2},$$

$$A_{24} = \left(\frac{V_{S_1}}{V_{P_0}}\right)\sin\theta,$$

the elements of the third row are

$$A_{31} = 2\left(\frac{V_{S_0}^2}{V_{P_0}^2}\right)\sin\theta\left[1-\sin^2\theta\right]^{1/2},$$

$$A_{32} = \left(\frac{V_{S_0}}{V_{P_0}}\right)\left[1 - 2\left(\frac{V_{S_0}^2}{V_{P_0}^2}\right)\sin^2\theta\right],$$

$$A_{33} = 2\left(\frac{\rho_1}{\rho_0}\right)\left(\frac{V_{S_1}^2}{V_{P_0}^2}\right)\sin\theta\left[1 - \left(\frac{V_{P_1}^2}{V_{P_0}^2}\right)\sin^2\theta\right]^{1/2},$$

$$A_{34} = -\left(\frac{\rho_1}{\rho_0}\right)\left(\frac{V_{S_1}}{V_{P_0}}\right)\left[1 - 2\left(\frac{V_{S_1}^2}{V_{P_0}^2}\right)\sin^2\theta\right],$$

the elements of the fourth row are

$$A_{41} = -\left[1 - 2\left(\frac{V_{S_0}^2}{V_{P_0}^2}\right)\sin^2\theta\right],$$

$$A_{42} = 2\left(\frac{V_{S_0}^2}{V_{P_0}^2}\right)\sin\theta\left[1 - \left(\frac{V_{S_0}^2}{V_{P_0}^2}\right)\sin^2\theta\right]^{1/2},$$

$$A_{43} = \left(\frac{\rho_1}{\rho_0}\right)\left(\frac{V_{P_1}}{V_{P_0}}\right)\left[1 - 2\left(\frac{V_{S_1}^2}{V_{P_0}^2}\right)\sin^2\theta\right],$$

$$A_{44} = 2\left(\frac{\rho_1}{\rho_0}\right)\left(\frac{V_{S_1}^2}{V_{P_0}^2}\right)\sin\theta\left[1 - \left(\frac{V_{S_1}^2}{V_{P_0}^2}\right)\sin^2\theta\right]^{1/2},$$

and the elements of the vector on the right-hand side are

$$b_1 = \sin\theta,$$

$$b_2 = \left[1-\sin^2\theta\right]^{1/2},$$

$$b_3 = 2\left(\frac{V_{S_0}^2}{V_{P_0}^2}\right)\sin\theta\left[1-\sin^2\theta\right]^{1/2},$$

$$b_4 = \left[1 - 2\left(\frac{V_{S_0}^2}{V_{P_0}^2}\right)\sin^2\theta\right].$$

Since we are interested in determining values for $R_{\mathrm{PP}}(\theta)$, Cramer's rule will be implemented by taking the determinant of the 4x4 matrix and dividing it by the augmented matrix. In practice this calculation can be unstable and may not be practical. In regards to real

world data, $R_{\text{PP}}(\theta)$ contains an abundance of noise as angle or offset increases and thus data at large angles are typically ignored. This has led authors such as Aki and Richards (2002) to derive an approximation to the Zoeppritz equations. Today, many different AVO methods have been developed in conjunction with Aki and Richards (2002) (Shuey, 1985; Ostrander, 1984; Gray et al., 1999; Smith and Gidlow, 1987; Castagna et al., 1998). Another method of linearizing the Zoeppritz equations is to define a perturbation. In the context of AVO, this perturbation quantifies the contrast in acoustic changes in the same way reflectivity, such as $\frac{\Delta V_P}{V_P}$, quantifies a change in P-wave velocity. Just as Aki and Richards (2002) describes contrasts in the form of a $\Delta x/x$, they use three measurements of contrast; those measuring changes in V_P, V_S, and ρ. In the following section we also choose three measurements but instead for poroelastic properties in conjunction with implementing these properties into the Zoeppritz equations. After defining these poroelastic property contrasts or perturbations in this case, we can substitute them into the Zoeppritz equations and expand each element using a Taylor series expansion which eliminates radical and fractional expressions. This is shown in more detail by Innanen (2011b). In doing so, we can approximate an expression for R_{PP} and truncate where necessary to derive an expression in the same scope as Aki and Richards (2002). As our approximation will be lending model parameters from Russell et al. (2011), Russell and Gray's AVO equation will be used for analytical comparison. The model parameters will be in terms of a perturbation which will measure fluid (a_f), shearing motion (a_μ), and density (a_μ). Noting that each perturbation is for the saturated case.

RUSSELL AND GRAY'S APPROXIMATION

As Russell et al. (2011) has demonstrated, the authors have devised a linearized approximation for PP reflection coefficients that is comparable to Aki and Richards (2002) derivation. This derivation follows suit with other previously derived AVO formulas (Shuey, 1985; Smith and Gidlow, 1987; Fatti et al., 1994) where weighting coefficients, that are functions of angle, characteristically determine the amplitude of a PP reflection. This formulation as shown by Russell et al. (2011) also shows a more direct way of detecting fluid in the target medium. One way of expressing a PP reflection is shown by

$$R^{(\text{Ru})}(\theta') \approx \left[\left(1 - \frac{\left(\gamma'_{\text{dry}}\right)^2}{\left(\gamma'_{\text{sat}}\right)^2}\right)\frac{\sec^2\theta'}{4}\right]\frac{\Delta f}{f} + \left[\frac{\left(\gamma'_{\text{dry}}\right)^2}{4\left(\gamma'_{\text{sat}}\right)^2}\sec^2\theta' - \frac{2}{\left(\gamma'_{\text{sat}}\right)^2}\sin^2\theta'\right]\frac{\Delta\mu}{\mu} + \left[\frac{1}{2} - \frac{\sec^2\theta'}{4}\right]\frac{\Delta\rho}{\rho}, \tag{9}$$

where: θ' is the average between the incidence and refraction angles, $\frac{\Delta f}{f}$, $\frac{\Delta\mu}{\mu}$, and $\frac{\Delta\rho}{\rho}$ are the reflectivities, $\gamma'_{\text{sat}} = (V_{P_0} + V_{P_1})/(V_{S_0} + V_{S_1})$, and $\gamma'_{\text{dry}} = (V_{P_0} + V_{P_1})_{\text{dry}}/(V_{S_0} + V_{S_1})_{\text{dry}}$. 'Dry' refers to the skeletal framework or matrix surrounding the pores and 'sat' refers to in-situ information. These reflectivities are defined as

$$\frac{\Delta f}{f} = \frac{2(f_1 - f_0)}{f_1 + f_0}, \qquad \frac{\Delta\mu}{\mu} = \frac{2(\mu_1 - \mu_0)}{\mu_1 + \mu_0}, \qquad \frac{\Delta\rho}{\rho} = \frac{2(\rho_1 - \rho_0)}{\rho_1 + \rho_0}. \tag{10}$$

By inspection, equation (9) informs us of a few details about the subsurface. Here, we can see that the three parameters used for the modelling is based around a difference of

a lithological property divided by its average which are also called the reflectivities. The weighting coefficient for the fluid reflectivity is highly determined by the difference in V_P/V_S ratios from the dry framework to the in-situ. The second weighting term in the equation provides some insight just as the first term does and is also dependent on the V_P/V_S ratios. The density reflectivity weighting term is simply driven by angle.

Re-writing the Zoeppritz equations in terms of poroelasticity

Just as Aki and Richards (2002) and Russell et al. (2011) have derived AVO approximations by defining reflectivities in terms of a difference of the medium contrast divided by the average, such as $\Delta\alpha/\alpha$ (Aki and Richards, 2002), we will similarly define a contrast in terms of perturbation notation. As mentioned previously, we will use three perturbations in fluid, shear modulus, and density which will be defined as

$$a_f = 1 - \frac{f_0}{f_1}, \qquad a_\mu = 1 - \frac{\mu_0}{\mu_1}, \qquad a_\rho = 1 - \frac{\rho_0}{\rho_1}. \tag{11}$$

In order to change the dependency in the Zoeppritz equations from elastic to poroelastic, that change will be made through making substitutions of the velocity and density ratios in equation (8). For the V_S ratio, equations (1), (2), and (11) show that

$$\left(\frac{V_{S_1}^2}{V_{S_0}^2}\right) = \left(\frac{\mu_1}{\rho_1}\right)\left(\frac{\rho_0}{\mu_0}\right) = (1-a_\mu)^{-1}(1-a_\rho). \tag{12}$$

For ρ, we will define its ratio such that

$$\left(\frac{\rho_1}{\rho_0}\right) = (1-a_\rho)^{-1}. \tag{13}$$

Finally for a V_P ratio, we will define it as

$$\left(\frac{V_{P_1}^2}{V_{P_0}^2}\right) = (1-a_\rho)\left[\left(\frac{\gamma_{\text{dry}}^2}{\gamma_{\text{sat}}^2}\right)(1-a_\mu)^{-1} + \left(1-\frac{\gamma_{\text{dry}}^2}{\gamma_{\text{sat}}^2}\right)(1-a_f)^{-1}\right], \tag{14}$$

where $\gamma_{\text{sat}} = (V_{P_0}/V_{S_0})_{\text{sat}}$ and $\gamma_{\text{dry}} = (V_{P_0}/V_{S_0})_{\text{dry}}$. These terms are extracted from Russell et al. (2011). The details of this derivation is found in the appendix. With these ratios, we may show the result of substituting equations (12)-(14) into (8), use Cramer's rule, and truncate.

Recovery of Russell and Gray's approximation

The resulting first order poroelastic AVO approximation for a PP reflection is

$$\begin{aligned} R^{(1)}(\theta) \approx & \left[\frac{1}{4}\left(1+\sin^2\theta\right) - \frac{\gamma_{\text{dry}}^2}{4\gamma_{\text{sat}}^2}\left(1+\sin^2\theta\right)\right] a_f \\ & + \left[\frac{\gamma_{\text{dry}}^2}{4\gamma_{\text{sat}}^2}\left(1+\sin^2\theta\right) - \frac{2}{\gamma_{\text{sat}}^2}\sin^2\theta\right] a_\mu + \left[\frac{1}{4} - \frac{\sin^2\theta}{4}\right] a_\rho. \end{aligned} \tag{15}$$

The coefficients displayed in equation (15) may be simplified further by using trigonometric properties of small angle. Since this is the case for AVO, we will use a small angle approximation where $1 + \sin^2\theta \approx \sec^2\theta$. This is shown by the trigonometric relationship of

$$\sec^2\theta = \frac{1}{\cos^2\theta} = \frac{1}{1-\sin^2\theta} = 1 + \sin^2\theta + \sin^4\theta + ... \tag{16}$$

This will allow us to write our first order poroelastic reflection coefficient approximation as

$$\begin{aligned} R^{(1)}(\theta) \approx & \left[\left(1 - \frac{\gamma^2_{\text{dry}}}{\gamma^2_{\text{sat}}}\right)\frac{\sec^2\theta}{4}\right] a_f + \left[\frac{\gamma^2_{\text{dry}}}{4\gamma^2_{\text{sat}}}\sec^2\theta - \frac{2}{\gamma^2_{\text{sat}}}\sin^2\theta\right] a_\mu \\ & + \left[\frac{1}{2} - \frac{\sec^2\theta}{4}\right] a_\rho. \end{aligned} \tag{17}$$

Equation (17) shows many similarities to Russell and Gray's $f - m - r$ (fluid-mu-rho) equation which is described by equation (9). It is interesting to note that the first order poroelastic AVO equation is nearly identical to Russell and Gray's $f - m - r$ equation. This is because both equations have been derived differently where the first order poroelastic AVO equation is derived through Zoeppritz and the $f - m - r$ equation is derived from the Aki and Richards equation. Since the Aki and Richards equation is also derived from Zoeppritz, equations (17) and (9) must be equivalent. Between these two equations, there are three differences. Those being which poroelastic modelling parameters are used ($a_x \leftrightarrow \frac{\Delta x}{x}$), angle ($\theta \leftrightarrow \theta'$), and ($\gamma \leftrightarrow \gamma'$). In the following, the first two differences will show to have equivalence when dealing with small contrasts. The third difference involving γ is outlined by Russell et al. (2003) and provides a better understanding of the velocity ratio. We do not explicitly show here an equivalence between γ and γ' but a comparison from the resulting conclusions made at the end of this section with Russell and Gray's $f - m - r$ is interesting to note. To continue, showing equivalence between equations (17) and (9), $\theta \equiv \theta'$ by a small angle approximation between two media as that is important for perturbation analysis. From above, $\sin^2\theta'$ may be written as

$$\sin^2\theta' = \sin^2\left(\frac{\theta_0 + \theta_1}{2}\right), \tag{18}$$

where θ_0 is the incidence angle and $\theta_1 = \sin^{-1}\left(\frac{V_{P_1}}{V_{P_0}}\sin\theta_0\right)$ which is the refracted angle using Snell's law. Substituting θ_1 into equation (18) and remembering that we are assuming small angles and small contrasts yields

$$\sin^2\theta' = \sin^2\left(\frac{\theta_0}{2} + \frac{1}{2}\sin^{-1}\left(\frac{V_{P_1}}{V_{P_0}}\sin\theta_0\right)\right) \approx \sin^2\left(\frac{\theta_0}{2} + \frac{\theta_0}{2}\right) = \sin^2\theta_0. \tag{19}$$

The same is true for $\sec^2\theta'$. Second, to show that $a_f \equiv \frac{\Delta f}{f}$ will require equation (10) where small contrasts will again be assumed. Writing this explicitly for $\frac{\Delta f}{f}$, we note that

$$\begin{aligned} \frac{\Delta f}{f} &= \frac{2(f_1 - f_0)}{f_1 + f_0} = 2\frac{1 - \frac{f_0}{f_1}}{1 + \frac{f_0}{f_1}} = 2\frac{a_f}{1 + (1 - a_f)} \\ &= \frac{a_f}{1 - \frac{1}{2}a_f} = a_f\left[1 + \left(\frac{1}{2}a_f\right) + \left(\frac{1}{2}a_f\right)^2 + ...\right] \approx a_f. \end{aligned} \tag{20}$$

This is also known as series reversion up to first order. By inspection, linearizations of the other reflectivities, $\frac{\Delta\mu}{\mu}$ and $\frac{\Delta\rho}{\rho}$, will also result in the same way where $\frac{\Delta x}{x} \approx a_x$. Thus the forms of equations (17) and (9) are equivalent. This also shows that the $f-m-r$ equation is also of first order. As we have shown a series reversion from the reflectivity domain into the perturbation domain as shown in equation (20) in order to compare the first order poroelastic equation and the $f-m-r$ equation, the same maneuver can be performed vice versa where we can find an expression for perturbation in terms of reflectivity constants. Just as it was shown using the fluid reflectivity, the same will be done here for visual consistency but the same method is performed on the other reflectivities. Here we will provide a more explicit description of series reversion using the fluid reflectivity. The fluid reflectivity as shown by equation (20) or the forward series in this case is written in terms of perturbations such that

$$\frac{\Delta f}{f} = a_f + \frac{1}{2}a_f^2 + ... \tag{21}$$

and perturbation, or the inverse series, is written as

$$a_f = a_{f_1} + a_{f_2} + ... \tag{22}$$

By substituting (22) into (21) and then equating like orders, a new expression for equation (22) is written as

$$a_f = \frac{\Delta f}{f} - \frac{1}{2}\left(\frac{\Delta f}{f}\right)^2 + ... \tag{23}$$

which describes fluid perturbation in terms of fluid reflectivity. Thus it is also true that

$$a_\mu = \frac{\Delta \mu}{\mu} - \frac{1}{2}\left(\frac{\Delta \mu}{\mu}\right)^2 + ..., \tag{24}$$

and

$$a_\rho = \frac{\Delta \rho}{\rho} - \frac{1}{2}\left(\frac{\Delta \rho}{\rho}\right)^2 + ... \tag{25}$$

By replacing these definitions for perturbations back into the Zoeppritz equations as done previously, then apply a Taylor expansion, truncate up to first order terms, and perform Cramer's rule, the first order approximation will result in

$$\begin{aligned} R^{(1)}(\theta) \approx & \left[\left(1 - \frac{\gamma_{\text{dry}}^2}{\gamma_{\text{sat}}^2}\right)\frac{\sec^2\theta}{4}\right]\frac{\Delta f}{f} + \left[\frac{\gamma_{\text{dry}}^2}{4\gamma_{\text{sat}}^2}\sec^2\theta - \frac{2}{\gamma_{\text{sat}}^2}\sin^2\theta\right]\frac{\Delta\mu}{\mu} \\ & + \left[\frac{1}{2} - \frac{\sec^2\theta}{4}\right]\frac{\Delta\rho}{\rho}, \end{aligned} \tag{26}$$

which has the same form as the $f-m-r$ equation.

Non-linear poroelastic AVO

This can be extended into higher orders to correct for errors that the linear correction is not able to account for. To do this only requires a change in the number of terms to be truncated at the Taylor expansion stage as shown in equation (20). The reflection coefficient that is corrected for linear and second order terms will have the form of

$$\begin{aligned} R^{(2)}(\theta) \approx & \underbrace{W_{a_1}a_f + W_{a_2}a_\mu + W_{a_3}a_\rho}_{1^{st}order} \\ & + \underbrace{W_{a_4}a_f^2 + W_{a_5}a_\mu^2 + W_{a_6}a_\rho^2 + W_{a_7}a_f a_\mu + W_{a_8}a_f a_\rho + W_{a_9}a_\mu a_\rho}_{2^{nd}order}, \end{aligned} \tag{27}$$

where the weighting coefficients are shown in the appendix. This we will denote as the second order poroelastic AVO equation. Just as we have displayed the second order approximation in terms of perturbations, the reflectivity approximation has the same form as equation (27) where

$$\begin{aligned} R^{(2)}(\theta) \approx & W_{\Delta_1}\frac{\Delta f}{f} + W_{\Delta_2}\frac{\Delta \mu}{\mu} + W_{\Delta_3}\frac{\Delta \rho}{\rho} + W_{\Delta_4}\left(\frac{\Delta f}{f}\right)^2 + W_{\Delta_5}\left(\frac{\Delta \mu}{\mu}\right)^2 \\ & + W_{\Delta_6}\left(\frac{\Delta \rho}{\rho}\right)^2 + W_{\Delta_7}\frac{\Delta f}{f}\frac{\Delta \mu}{\mu} + W_{\Delta_8}\frac{\Delta f}{f}\frac{\Delta \rho}{\rho} + W_{\Delta_9}\frac{\Delta \mu}{\mu}\frac{\Delta \rho}{\rho}, \end{aligned} \tag{28}$$

where its weighting terms are also found in the appendix. There are many similarities between this derivation and the derivation that uses perturbation notation. By inspection, weighting terms 1-3 and 7-9 are identical between equations (27) and (28) which leaves 4-6 to be different. This difference is most likely explained by the nature in which the process of expanding the rational and fractional terms in equation (8) carries out the arithmetic of the Taylor expansion that happens to derive particular expressions for the weighting coefficients; for the linear cases, the weighting coefficients for equation (27) will be exactly the same as (28) because of a one-to-one change from perturbation to reflectivity. This however does not explain why weighting coefficients 7-9 are identical as shown by equation (20).

NUMERICAL RESULTS

The previous section shows several expressions in approximating reflectivity as it varies with angle for first, second, and third order variations using both perturbation models and reflectivity models. For numerical testing, the Zoeppritz equations will provide some visual measure of the performances of each approximation that was derived. Although no statistical measure is provided here that shows the competency of each approximation with respect to Zoeppritz, a visual inspection of these approximations in figure (6) shows qualitative comparisons. In the following figure, the first, second, and third order approximations using perturbation models are used in comparison with the Zoeppritz equations. In figure (6) the perturbation models start small and gradually increase. This is to demonstrate the behaviour of each approximations proximity to Zoeppritz. It is quite clear from this figure that the third order approximation performs with more accuracy in this regard and is a trend with various modelling parameters not shown here. In the next figure, we demonstrate the

Model parameters (a_f, a_μ, a_ρ)	values $\left(a_x = 1 - \frac{x_0}{x_1}\right)$
figure(6a)	0.1
figure(6b)	0.2
figure(6c)	0.4
figure(6d)	0.5

Table 1: Perturbation Models

same analysis but with reflectivity parameters. We can see in figure (7) that the reflectivity approximations exhibit much more accuracy than their perturbation counterparts. This will be better illustrated in the next subsection.

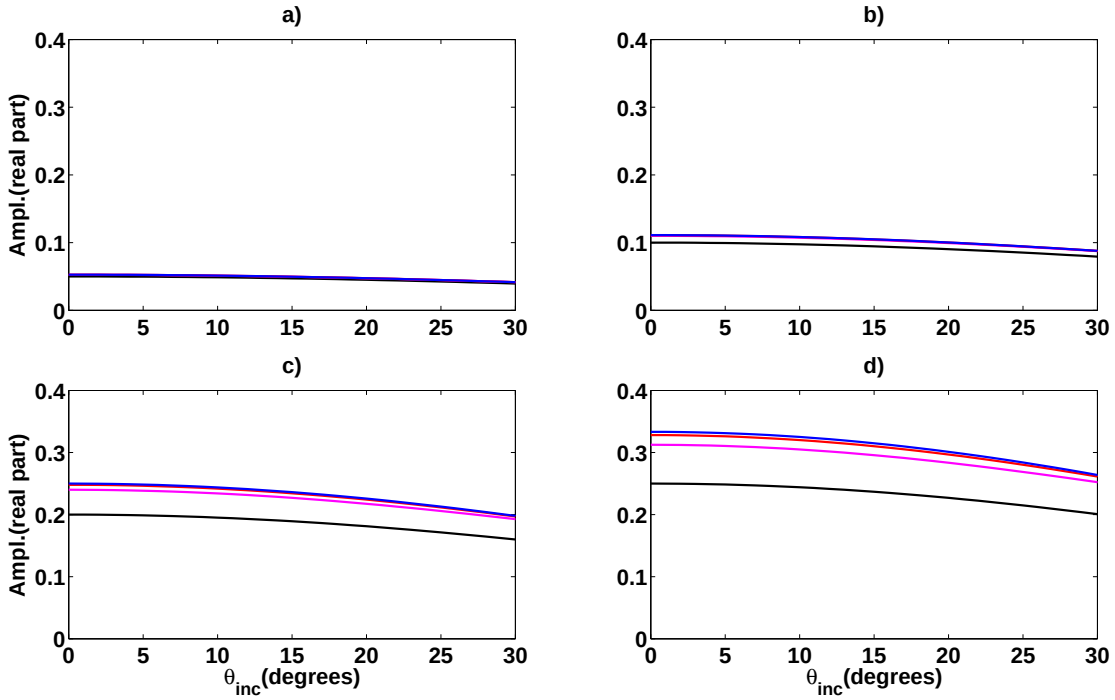

FIG. 6: All four panels have chosen a consistent perturbation each in a_f, a_μ, and a_ρ. The top left panel uses a perturbation of 0.1. Then it increases from one panel to the next in the top right panel to 0.2, 0.4 in the bottom left and 0.5 in the last panel. The blue curve represents synthetic data that is the Zoeppritz equations while the black curve represents the first order approximation, the magenta curve represents second order, and the red curve represents third order.

Model parameters $\left(\frac{\Delta f}{f}, \frac{\Delta \mu}{\mu}, \frac{\Delta \rho}{\rho}\right)$	values $\left(\frac{\Delta x}{x} = \frac{2(x_1 - x_0)}{x_1 + x_0}\right)$
figure(7a)	0.1
figure(7b)	0.2
figure(7c)	0.4
figure(7d)	0.5

Table 2: Reflectivity Models

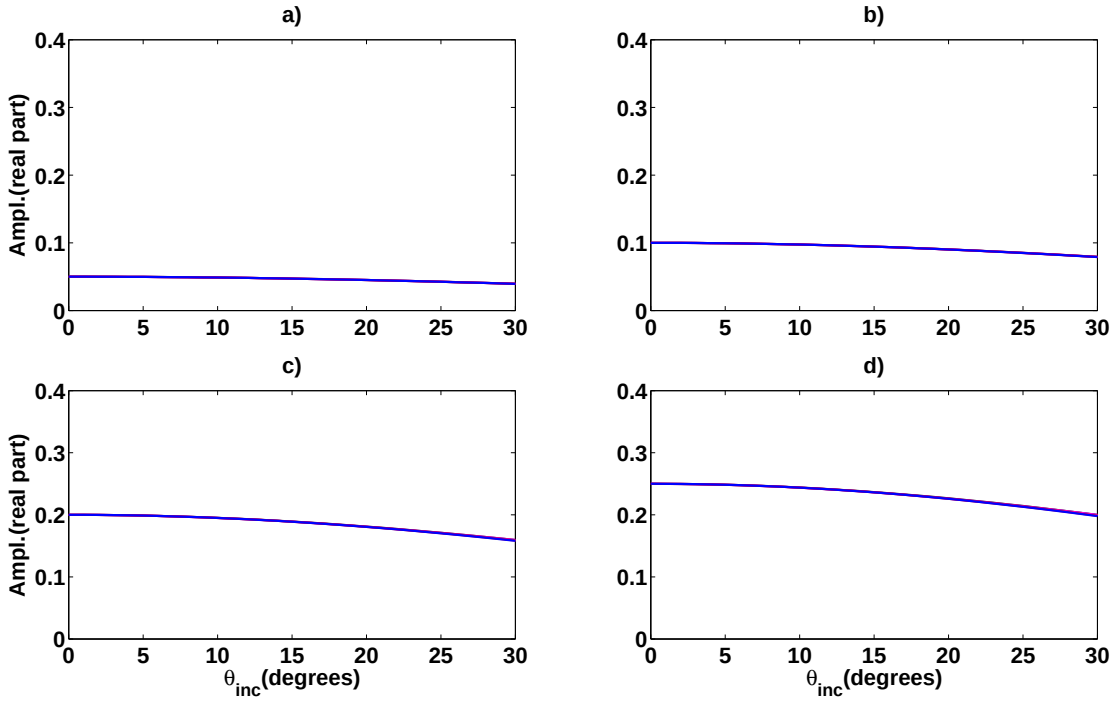

FIG. 7: All four panels have chosen a consistent reflectivity each in $\frac{\Delta f}{f}$, $\frac{\Delta \mu}{\mu}$, and $\frac{\Delta \rho}{\rho}$. The values of the reflectivity models mirrors the values from the previous figure as well as the curves for comparison.

A more extensive comparison between perturbation and reflectivity approximations

Based on the results of the previous section, the reflectivity approximations are able to account for larger contrasts than the perturbation approximations. The following work will show how each perturbation/reflectivity parameter affects its corresponding poroelastic AVO approximation. A side by side comparison between each model will be shown where one model parameter is adjusted while the others remain fixed to illustrate a larger bias of the weighting parameter it is coupled to. Equation (**??**) demonstrates how the parameters were calculated. In figure (8), we have chosen to use perturbation and reflectivity model values of 0.3 and tables () and () show how this parameter is used to observe the amplitude variation effects caused by this value. Using a value of 0.3 for fluid contrasts in the perturbation and reflectivity domains appears to not exhibit any amplitude changes for angles up to approximately 20° for the incidence angle and is shown in figures (a) and (b); in addition there also appears to be a sloping upwards as measured amplitudes approach the critical angle. For shear modulus contrasts of 0.3, AVO effects are more pronounced for shallower angles and this is shown in figures (c) and (d). The 1st order approximation

has a noticeable drop off in accuracy with respect to the 2nd and 3rd order approximations which is also apparent when fluid contrasts are 0.3. These approximations also indicate a sloping upwards of amplitudes as angle approaches critical. For density contrasts of 0.3 in the perturbation and reflectivity domains, a negative sloping AVO effect occurs.

In figure (9), the same form of analysis is performed but instead uses a contrast of 0.6 instead of 0.3 as used previously. Similarities between figures (8) and (9) are shown by the general AVO trends that are occurring. The main differences lie in the performances of the approximations where a more significant drop-off in amplitude is displayed by the 1st order approximation in figure (9a) - (9f) by the black curve with respect to the second and third order approximations. Figure (10) shows how a 0.9 contrast value affects the AVO curves. For fluid perturbation in (a), the higher order approximations does not significantly increase the amplitudes to match the elastic equations. In figures (10c) and (10e), shear modulus and density perturbations also show a lack of amplitude compensation in the higher orders but the reflectivities are closer to the Zoeppritz equations in (10b), (10d), and (10f).

$$f_0 = f_1(1 - a_f) = f_1\left(1 - \frac{\Delta f}{f}\left(1 + \frac{1}{2}\frac{\Delta f}{f}\right)^{-1}\right) \quad f_1 = 7.000GPa$$

$$\mu_0 = \mu_1(1 - a_\mu) = \mu_1\left(1 - \frac{\Delta \mu}{\mu}\left(1 + \frac{1}{2}\frac{\Delta \mu}{\mu}\right)^{-1}\right) \quad \mu_1 = 3.000GPa$$

$$\rho_0 = \rho_1(1 - a_\rho) = \rho_1\left(1 - \frac{\Delta \rho}{\rho}\left(1 + \frac{1}{2}\frac{\Delta \rho}{\rho}\right)^{-1}\right) \quad \rho_1 = 2.200g/cm^3$$

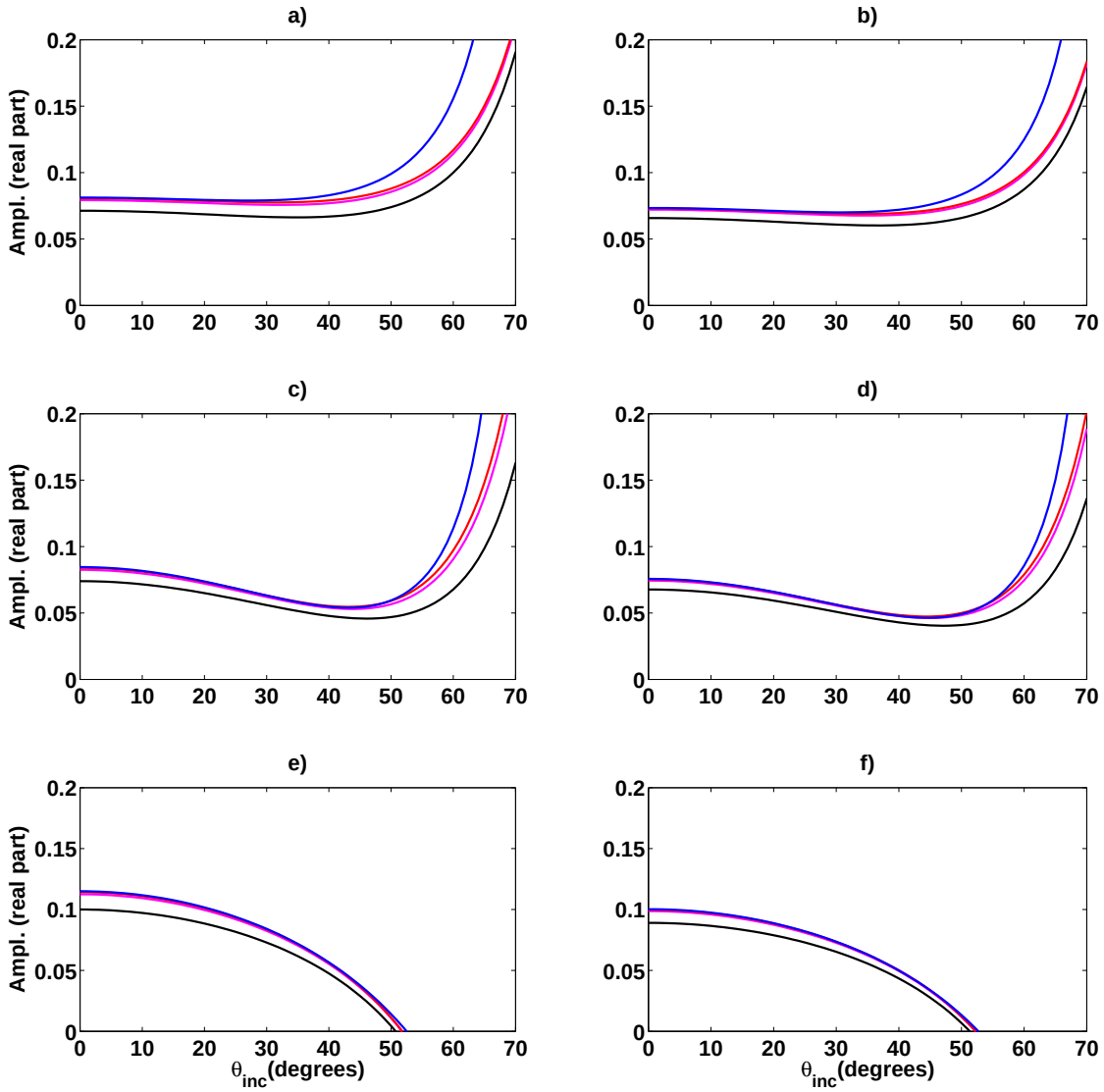

FIG. 8: (a), (c), (e) represent the perturbation poroelastic AVO approximations of 1st, 2nd, and 3rd order and are reflected by the black, magenta, and red curves respectively. (b), (d), and (f) represent the reflectivity poroelastic AVO approximations of 1st, 2nd, and 3rd order and are reflected by the black, magenta, and red curves respectivly. The elastic amplitudes are shown in the blue curve.

	a_f	a_μ	a_ρ
figure(8a)	0.3	0.1	0.1
figure(8c)	0.1	0.3	0.1
figure(8e)	0.1	0.1	0.3

Perturbation Models

	$\Delta f/f$	$\Delta\mu/\mu$	$\Delta\rho/\rho$
figure(8b)	0.3	0.1	0.1
figure(8d)	0.1	0.3	0.1
figure(8f)	0.1	0.1	0.3

Reflectivity Models

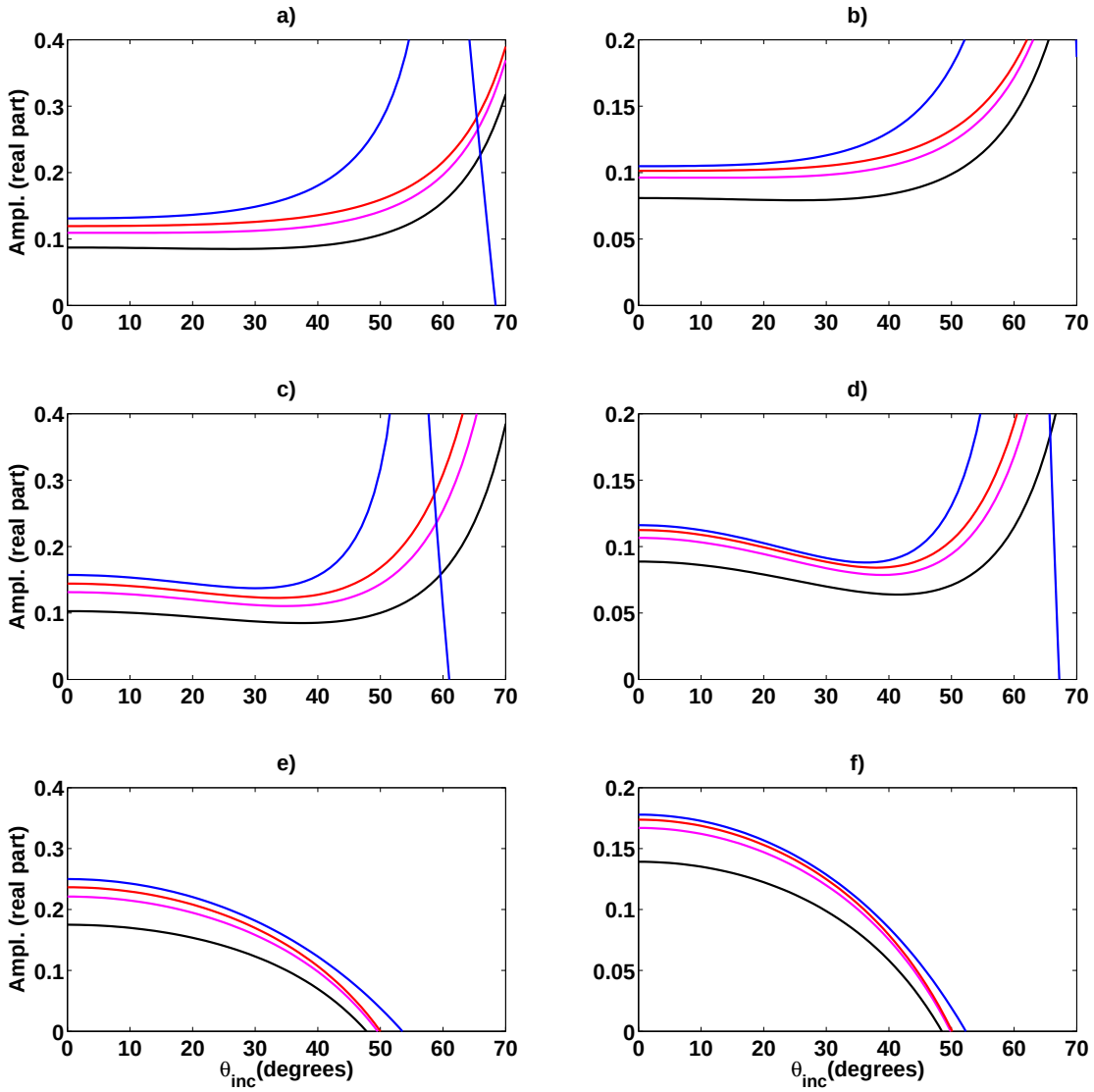

FIG. 9: (a), (c), (e) represent the perturbation poroelastic AVO approximations of 1st, 2nd, and 3rd order and are reflected by the black, magenta, and red curves respectively. (b), (d), and (f) represent the reflectivity poroelastic AVO approximations of 1st, 2nd, and 3rd order and are reflected by the black, magenta, and red curves respectivly. The elastic amplitudes are shown in the blue curve.

	a_f	a_μ	a_ρ
figure(9a)	0.6	0.1	0.1
figure(9c)	0.1	0.6	0.1
figure(9e)	0.1	0.1	0.6

Perturbation Models

	$\Delta f/f$	$\Delta\mu/\mu$	$\Delta\rho/\rho$
figure(9b)	0.6	0.1	0.1
figure(9d)	0.1	0.6	0.1
figure(9f)	0.1	0.1	0.6

Reflectivity Models

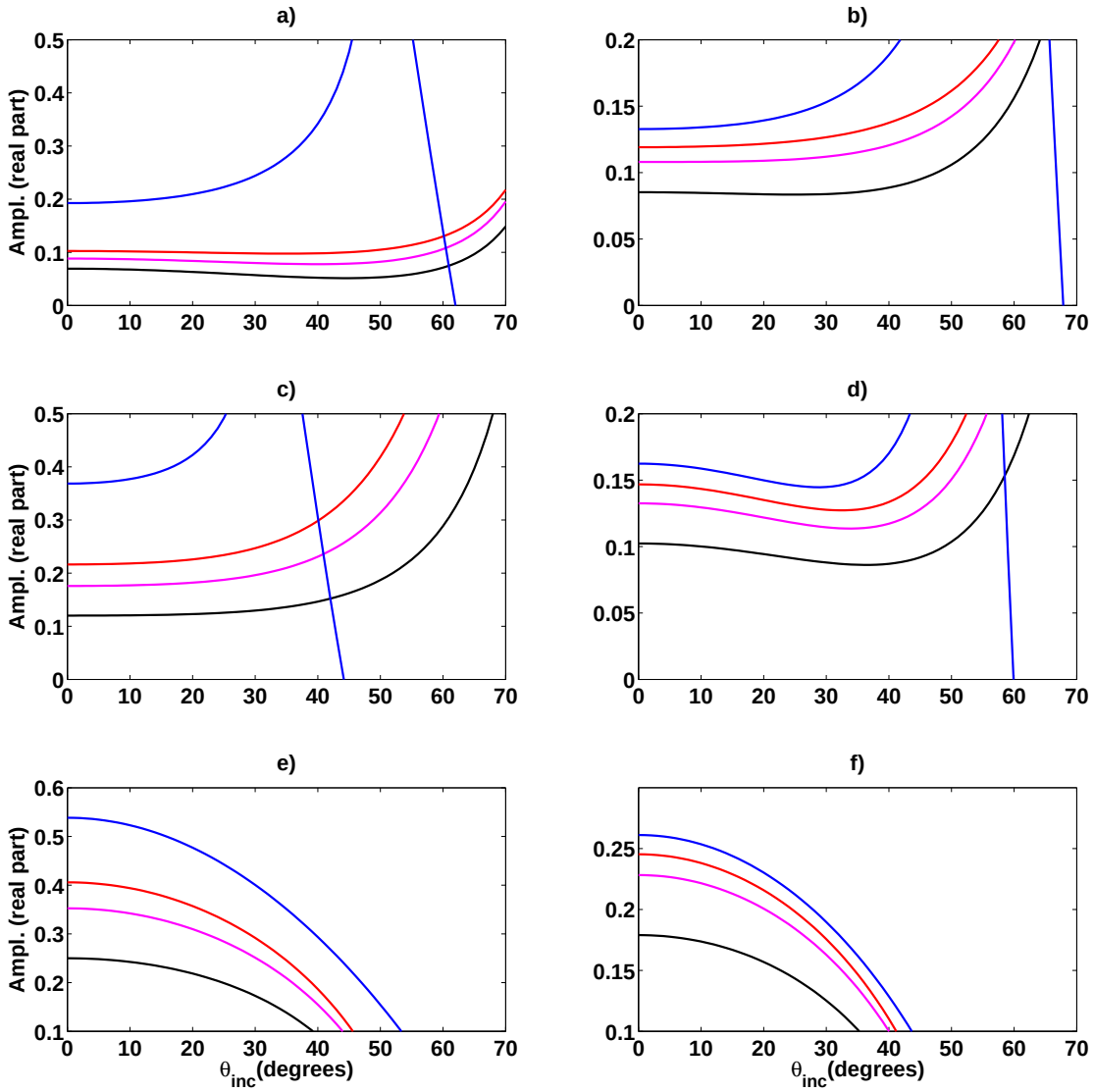

FIG. 10: (a), (c), (e) represent the perturbation poroelastic AVO approximations of 1st, 2nd, and 3rd order and are reflected by the black, magenta, and red curves respectively. (b), (d), and (f) represent the reflectivity poroelastic AVO approximations of 1st, 2nd, and 3rd order and are reflected by the black, magenta, and red curves respectivly. The elastic amplitudes are shown in the blue curve.

	a_f	a_μ	a_ρ
figure(10a)	0.9	0.1	0.1
figure(10c)	0.1	0.9	0.1
figure(10e)	0.1	0.1	0.9

Perturbation Models

	$\Delta f/f$	$\Delta\mu/\mu$	$\Delta\rho/\rho$
figure(10b)	0.9	0.1	0.1
figure(10d)	0.1	0.9	0.1
figure(10f)	0.1	0.1	0.9

Reflectivity Models

Effects of γ^2_{dry} on linear coefficients

In addition to the investigation of the manner in which the poroelastic AVO approximations change as we change the model parameters, another influence of these AVO curves results from changing the γ^2_{dry} term. This term is described as a dialing mechanism by Russell et al. (2011) that describes the skeleton V_P/V_S ratio. But how does this effect our AVO approximations? As we have just seen, fluid perturbation for large contrasts does not significantly improve the prediction of the third order approximation relative to the 1st order approximation. This may depend on what γ^2_{dry} value is calculated based on the petrophysical parameters. In the following figure, we can see how the weighting coefficients are affected by selecting petrophysical parameters that show a range of γ^2_{dry} values. These values are provided by Russell et al. (2011). Since the 1st order weighting coefficients provide the most clarity relative to the non-linear weights, we will analyze these. Figure (11) uses 8 different γ^2_{dry} values to calculate 8 different sets of weighting coefficients for the 1st order weights. We would also like to note that the γ^2_{sat} term is kept constant. In figure (11a), the fluid perturbation weight is constant because both γ^2_{dry} and γ^2_{sat} are equal. As γ^2_{dry} decreases, the shear modulus perturbation weight and the fluid perturbation weight begin to converge at normal incidence also noting that the density perturbation weight does not change because it is not dependent on γ^2_{dry}.

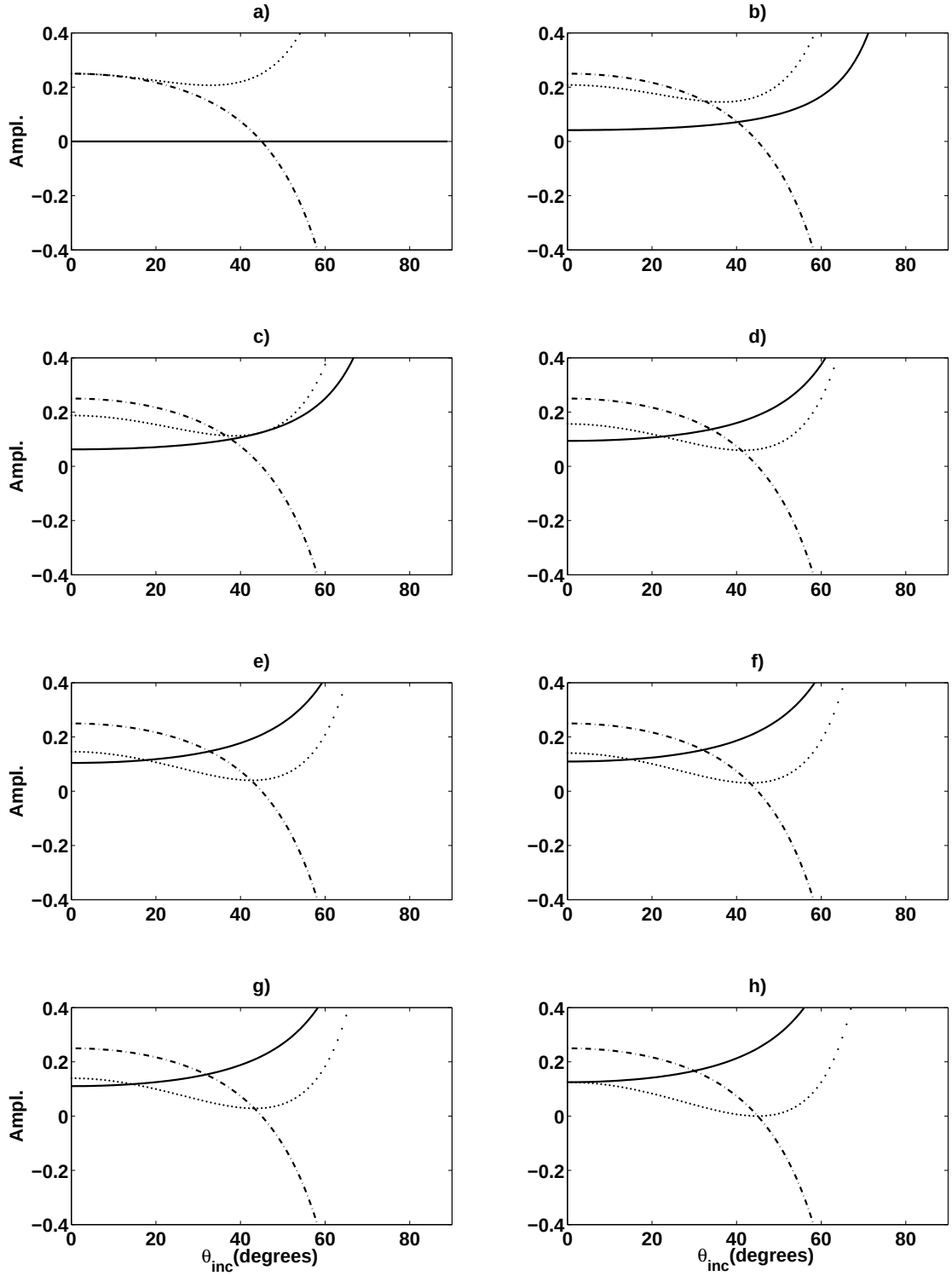

FIG. 11: Figures (a)-(h) show weighting coefficients $W_{a_1} = W_{\Delta_1}$, $W_{a_2} = W_{\Delta_2}$, and $W_{a_3} = W_{\Delta_3}$ for γ^2_{dry} values of 4.000, 3.333, 3.000, 2.500, 2.333, 2.250, 2.233, and 2.000 respectively each with a base γ^2_{sat} value of 4.000. The solid black line, dotted line, and dashed-dotted line represent W_{a_1}, W_{a_2}, and W_{a_3} respectively.

DISCUSSION

As Innanen (2011b) has shown equivalent forms between first order elastic AVO and the Aki-Richards equation, this has also occurred for the poroelastic case. Of the six poroelastic AVO equations, the reflectivity models showed a numerical significance. The significance of this result shows that these approximations have wider numerical variability although more testing needs to be done using geophysically realistic values. Between the perturbation second order equation and the reflectivity second order equation, the weighting terms are nearly identical. The subtle differences are encapsulated inside weights 4-6 which are the squared terms. At larger angles, $\theta > 30°$, a cusp that is indicative of non-linear variation occurs (Innanen, 2011c). As medium properties change more drastically from the incident medium to the target medium, the more significant the non-linear effects occur which causes greater instability of the poroelastic approximations. This is a phenomena that is demonstrated by the Zoeppritz equations as it is itself non-linear. Although non-linearity may hinder the results of a linear inversion, in the case for AVO inversion as performed in industry, data from higher angles are typically unused and thus extraction of rock information from small angles is viable.

CONCLUSION

This report is a demonstration of an analytical approach in understanding AVO inversion and its robustness using some basic numerical models. This approach shows a derivation of a poroelastic AVO approximation in terms of perturbation and reflectivity models. Research provided by Russell et al. (2011), Gray et al. (1999), and Shuey (1985) are frameworks in the observations and analysis that has been performed in this report. The poroelastic approximations that are shown here are based off of the Zoeppritz equations that is provided by Keys (1989) and have been shown to have significance for small angle reflections. There are two sets of approximations that have been derived, one using perturbation models to simulate incidence medium and target medium contrasts as $a_x = 1 - \frac{x_0}{x_1}$ and the other using reflectivity models where $\frac{\Delta x}{x} = \frac{2(x_1 - x_0)}{x_1 + x_0}$. For each set of approximations, a linear (first order) as well as non-linear (second and third order) forms have been derived from the Zoeppritz equations. The first order approximation shows to have the same form as Russell and Gray's $f - m - r$ equation. As predicted out of the six approximations, the third order approximation is the most stable in regards to amplitude replication where the second and first order approximations struggle more so in their respective capacities for both perturbation and reflectivity models. A repeated exercise of linear inversions using synthetic amplitudes to compare the perturbation models and reflectivity models was also demonstrated where the reflectivity approximation showed more stability.

ACKNOWLEDGMENTS

This work was funded by the CREWES Project and a University Research Award from Imperial Oil Limited. The authors gratefully acknowledge this support. We thank Brian Russell for valuable commentary and suggestions.

APPENDIX

The derivation for the V_P ratio as shown in equation (14) uses terminology borrowed by Russell et al. (2011). These terms include descriptions of the dry or empty pore matrix of the surrounding rock and the fluid term. The dry matrix is shown in equation (1) and fluid is quantified by

$$f = \rho V_P^2 - \gamma_{\text{dry}}^2 \mu \tag{A1}$$

By exploiting the fluid term definition, we can cancel some of the coupled density and velocity terms by the following:

$$\begin{aligned}
\left(\frac{V_{P_1}^2}{V_{P_0}^2}\right) &= \frac{s_1 + f_1}{\rho_1} \times \frac{\rho_0}{s_0 + f_0} \\
&= (1 - a_\rho)\left[\frac{s_1}{s_0 + f_0} + \frac{f_1}{s_0 + f_0}\right] \\
&= (1 - a_\rho)\left[\frac{\gamma_{\text{dry}}^2 \mu_1}{\rho_0 V_{P_0}^2} + \frac{f_0 (1 - a_f)^{-1}}{\rho_0 V_{P_0}^2}\right] \\
&= (1 - a_\rho)\left[\frac{\gamma_{\text{dry}}^2 \mu_0 (1 - a_\mu)^{-1}}{\rho_0 V_{P_0}^2} + \frac{(\rho_0 V_{P_0}^2 - \gamma_{\text{dry}}^2 \mu_0)(1 - a_f)^{-1}}{\rho_0 V_{P_0}^2}\right] \\
&= (1 - a_\rho)\left[\left(\frac{\gamma_{\text{dry}}^2}{\gamma_{\text{sat}}^2}\right)(1 - a_\mu)^{-1} + \left(1 - \frac{\gamma_{\text{dry}}^2}{\gamma_{\text{sat}}^2}\right)(1 - a_f)^{-1}\right].
\end{aligned} \tag{A2}$$

The coefficients for the second order poroelastic AVO equation with perturbation models are derived using software capable of mathematical computation and are as follows:

$$
\begin{aligned}
W_{a_1} &= \left(1 - \frac{\gamma_{\text{dry}}^2}{\gamma_{\text{sat}}^2}\right) \frac{\sec^2\theta}{4}, \\
W_{a_2} &= \frac{\gamma_{\text{dry}}^2}{4\gamma_{\text{sat}}^2} \sec^2\theta - \frac{2}{\gamma_{\text{sat}}^2} \sin^2\theta, \\
W_{a_3} &= \frac{1}{2} - \frac{\sec^2\theta}{4}, \\
W_{a_4} &= \left(1 - \frac{\gamma_{\text{dry}}^2}{\gamma_{\text{sat}}^2}\right) \frac{\sin^2\theta}{4} + \frac{1}{8}\left(1 - \frac{\gamma_{\text{dry}}^4}{\gamma_{\text{sat}}^4}\right), \\
W_{a_5} &= \frac{\gamma_{\text{dry}}^2}{4\gamma_{\text{sat}}^2}\left(\sec^2\theta - \frac{\gamma_{\text{dry}}^2}{2\gamma_{\text{sat}}^2}\right) - \frac{2}{\gamma_{\text{sat}}^2}\left(1 - \frac{1}{2\gamma_{\text{sat}}}\right)\sin^2\theta, \\
W_{a_6} &= \frac{1}{8}\left(1 - \frac{2}{\gamma_{\text{sat}}}\sin^2\theta\right), \\
W_{a_7} &= -\frac{\gamma_{\text{dry}}^2}{4\gamma_{\text{sat}}^2}\left(1 - \frac{\gamma_{\text{dry}}^2}{\gamma_{\text{sat}}^2}\right), \\
W_{a_8} &= -\left(1 - \frac{\gamma_{\text{dry}}^2}{\gamma_{\text{sat}}^2}\right)\frac{\sin^2\theta}{4}, \\
W_{a_9} &= \frac{1}{\gamma_{\text{sat}}^2}\left(1 - \frac{\gamma_{\text{dry}}^2}{4}\right)\sin^2\theta.
\end{aligned}
$$

The coefficients for the second order poroelastic AVO equation with reflectivity models are shown as:

$$
\begin{aligned}
W_{\Delta_1} &= \left(1 - \frac{\gamma_{\text{dry}}^2}{\gamma_{\text{sat}}^2}\right)\frac{\sec^2\theta}{4},\\
W_{\Delta_2} &= \frac{\gamma_{\text{dry}}^2}{4\gamma_{\text{sat}}^2}\sec^2\theta - \frac{2}{\gamma_{\text{sat}}^2}\sin^2\theta,\\
W_{\Delta_3} &= \frac{1}{2} - \frac{\sec^2\theta}{4},\\
W_{\Delta_4} &= \frac{1}{8}\left(1 - \frac{\gamma_{\text{dry}}^2}{\gamma_{\text{sat}}^2}\right)\left(\sin^2\theta + \frac{\gamma_{\text{dry}}^2}{\gamma_{\text{sat}}^2}\right),\\
W_{\Delta_5} &= \frac{\gamma_{\text{dry}}^2}{8\gamma_{\text{sat}}^2}\left(\sec^2\theta - \frac{\gamma_{\text{dry}}^2}{\gamma_{\text{sat}}^2}\right) - \frac{1}{\gamma_{\text{sat}}^2}\left(1 - \frac{1}{\gamma_{\text{sat}}}\right)\sin^2\theta,\\
W_{\Delta_6} &= \left(1 - \frac{2}{\gamma_{\text{sat}}}\right)\frac{\sin^2\theta}{8},\\
W_{\Delta_7} &= -\frac{\gamma_{\text{dry}}^2}{4\gamma_{\text{sat}}^2}\left(1 - \frac{\gamma_{\text{dry}}^2}{\gamma_{\text{sat}}^2}\right),\\
W_{\Delta_8} &= -\left(1 - \frac{\gamma_{\text{dry}}^2}{\gamma_{\text{sat}}^2}\right)\frac{\sin^2\theta}{4},\\
W_{\Delta_9} &= \frac{1}{\gamma_{\text{sat}}^2}\left(1 - \frac{\gamma_{\text{dry}}^2}{4}\right)\sin^2\theta.
\end{aligned}
$$

Similarly, the equation form of the third order poroelastic AVO equation in perturbation terms follows the first and second orders. It's reflectivity counterpart also contains the same form but instead of a_f, a_μ, and a_ρ as shown in equation (A3), $\frac{\Delta f}{f}$, $\frac{\Delta \mu}{\mu}$, and $\frac{\Delta \rho}{\rho}$ are used. The third order approximation takes the form

$$
\begin{aligned}
R^{(3)}(\theta) \approx\ & W_{a_1}a_f + W_{a_2}a_\mu + W_{a_3}a_\rho + W_{a_4}a_f^2 + W_{a_5}a_\mu^2 + W_{a_6}a_\rho^2\\
&+ W_{a_7}a_f a_\mu + W_{a_8}a_f a_\rho + W_{a_9}a_\mu a_\rho + W_{a_{10}}a_f^3 + W_{a_{11}}a_\mu^3\\
&+ W_{a_{12}}a_\rho^3 + W_{a_{13}}a_f^2 a_\mu + W_{a_{14}}a_f^2 a_\rho + W_{a_{15}}a_\mu^2 a_f + W_{a_{16}}a_\mu^2 a_\rho\\
&+ W_{a_{17}}a_\rho^2 a_f + W_{a_{18}}a_\rho^2 a_\mu + W_{a_{19}}a_f a_\mu a_\rho,
\end{aligned}
\tag{A3}
$$

and its weighting coefficients are displayed as

$$W_{a_{10}} = \frac{1}{64}\left[5\left(1+3\sin^2\theta\right)\left(1-\frac{1}{5}\frac{\gamma_{\text{dry}}^4}{\gamma_{\text{sat}}^4}\right)+\frac{\gamma_{\text{dry}}^2}{\gamma_{\text{sat}}^2}\left(1-13\sin^2\theta\right)-5\frac{\gamma_{\text{dry}}^6}{\gamma_{\text{sat}}^6}\left(1-\frac{\sin^2\theta}{5}\right)\right],$$

$$W_{a_{11}} = \frac{5}{64}\frac{\gamma_{\text{dry}}^6}{\gamma_{\text{sat}}^6}\left(1-\frac{\sin^2\theta}{5}\right)+\frac{1}{4}\frac{\gamma_{\text{dry}}^2}{\gamma_{\text{sat}}^2}\sec^2\theta+\frac{7}{4}\frac{1}{\gamma_{\text{sat}}^3}\left(1-\frac{2}{7}\frac{\gamma_{\text{dry}}^2}{\gamma_{\text{sat}}^2}\right)\sin^2\theta$$
$$-\frac{2}{\gamma_{\text{sat}}^2}\left(1-\frac{1}{16}\frac{\gamma_{\text{dry}}^4}{\gamma_{\text{sat}}^4}\right)\sin^2\theta-\frac{1}{4}\frac{\gamma_{\text{dry}}^4}{\gamma_{\text{sat}}^4},$$

$$W_{a_{12}} = \frac{5}{64}\left(1+\frac{\sin^2\theta}{5}\right)-\frac{3}{16\gamma_{\text{sat}}}\sin^2\theta,$$

$$W_{a_{13}} = \frac{15}{64}\frac{\gamma_{\text{dry}}^6}{\gamma_{\text{sat}}^6}\left(1-\frac{\sin^2\theta}{5}\right)-\frac{\gamma_{\text{dry}}^2}{64\gamma_{\text{sat}}^2}\left(1+3\sin^2\theta\right)-\frac{7}{32}\frac{\gamma_{\text{dry}}^4}{\gamma_{\text{sat}}^4}\left(1-\frac{3}{7}\sin^2\theta\right)$$
$$-\frac{1}{4}\frac{\gamma_{\text{dry}}^2}{\gamma_{\text{sat}}^4}\left(1-\frac{\gamma_{\text{dry}}^2}{2\gamma_{\text{sat}}^2}\right)\sin^2\theta+\frac{1}{8\gamma_{\text{sat}}^2}\sin^2\theta,$$

$$W_{a_{14}} = \frac{\gamma_{\text{dry}}^2}{32\gamma_{\text{sat}}^2}\left(1+9\sin^2\theta\right)-\frac{\gamma_{\text{dry}}^4}{64\gamma_{\text{sat}}^4}\sec^2\theta-\frac{1}{64}\left(1+17\sin^2\theta\right),$$

$$W_{a_{15}} = \left(1-\frac{\gamma_{\text{dry}}^2}{\gamma_{\text{sat}}^2}\right)\left(\frac{\gamma_{\text{dry}}^2}{4\gamma_{\text{sat}}^4}-\frac{1}{2\gamma_{\text{sat}}^3}\right)\sin^2\theta-\frac{\gamma_{\text{dry}}^2}{4\gamma_{\text{sat}}^2}+\frac{31}{64}\frac{\gamma_{\text{dry}}^4}{\gamma_{\text{sat}}^4}\left(1-\frac{3}{31}\sin^2\theta\right)$$
$$-\frac{15}{64}\frac{\gamma_{\text{dry}}^6}{\gamma_{\text{sat}}^6}\left(1-\frac{\sin^2\theta}{5}\right),$$

$$W_{a_{16}} = \frac{5}{4\gamma_{\text{sat}}^2}\left(1+\frac{\gamma_{\text{dry}}^2}{5\gamma_{\text{sat}}^2}\right)\sin^2\theta-\frac{3}{4\gamma_{\text{sat}}^3}\left(1+\frac{\gamma_{\text{dry}}^2}{3\gamma_{\text{sat}}^{-1}}\right)\sin^2\theta-\frac{\gamma_{\text{dry}}^4}{64\gamma_{\text{sat}}^4}\sec^2\theta,$$

$$W_{a_{17}} = -\left(1-\frac{\gamma_{\text{dry}}^2}{\gamma_{\text{sat}}^2}\right)\left(\frac{1}{8\gamma_{\text{sat}}}+\frac{\sec^2\theta}{64}\right),$$

$$W_{a_{18}} = \frac{3}{8\gamma_{\text{sat}}^2}\left(1-\frac{\gamma_{\text{dry}}^2}{3\gamma_{\text{sat}}}\right)\sin^2\theta-\frac{1}{16\gamma_{\text{sat}}}\sin^2\theta-\frac{\gamma_{\text{dry}}^2}{64\gamma_{\text{sat}}^2}\sec^2\theta,$$

$$W_{a_{19}} = \left(1-\frac{\gamma_{\text{dry}}^2}{\gamma_{\text{sat}}^2}\right)\left(\frac{1}{4\gamma_{\text{sat}}^2}\sin^2\theta-\frac{\gamma_{\text{dry}}^2}{32\gamma_{\text{sat}}^2}\sec^2\theta\right).$$

Finally, the weighting coefficients for the 3rd order approximation in terms of reflectivity models are

$$
\begin{aligned}
W_{\Delta_{10}} &= \frac{1}{64}\left[3\left(1-\frac{\gamma_{\text{dry}}^4}{\gamma_{\text{sat}}^4}\right)\sin^2\theta - 3\frac{\gamma_{\text{dry}}^2}{\gamma_{\text{sat}}^2}\left(1+\frac{\sin^2\theta}{3}\right)+\left(1+7\frac{\gamma_{\text{dry}}^4}{\gamma_{\text{sat}}^4}\right)\right.\\
&\quad \left. - 5\frac{\gamma_{\text{dry}}^6}{\gamma_{\text{sat}}^6}\left(1-\frac{\sin^2\theta}{5}\right)\right],\\
W_{\Delta_{11}} &= \frac{5}{64}\frac{\gamma_{\text{dry}}^6}{\gamma_{\text{sat}}^6}\left(1-\frac{\sin^2\theta}{5}\right)-\frac{1}{2\gamma_{\text{sat}}^2}\left(1+\frac{\gamma_{\text{dry}}^2}{\gamma_{\text{sat}}^3}\right)\sin^2\theta+\frac{\gamma_{\text{dry}}^2}{16\gamma_{\text{sat}}^2}\sec^2\theta\\
&\quad -\frac{\gamma_{\text{dry}}^4}{8\gamma_{\text{sat}}^4}\left(1-\frac{\sin^2\theta}{\gamma_{\text{sat}}^2}\right)+\frac{3}{4\gamma_{\text{sat}}^3}\sin^2\theta,\\
W_{\Delta_{12}} &= \frac{1}{64}\left(1-3\sin^2\theta\right)+\frac{1}{16\gamma_{\text{sat}}}\sin^2\theta,\\
W_{\Delta_{13}} &= \frac{1}{8\gamma_{\text{sat}}^2}\sin^2\theta-\frac{3}{64}\frac{\gamma_{\text{dry}}^2}{\gamma_{\text{sat}}^2}\left(1+\frac{\gamma_{\text{dry}}^4}{\gamma_{\text{sat}}^4}\right)\sin^2\theta-\frac{\gamma_{\text{dry}}^2}{4\gamma_{\text{sat}}^4}\left(1-\frac{\gamma_{\text{dry}}^2}{2\gamma_{\text{sat}}^2}\right)\sin^2\theta\\
&\quad -\frac{11}{32}\frac{\gamma_{\text{dry}}^4}{\gamma_{\text{sat}}^4}\left(1-\frac{3}{11}\sin^2\theta\right)+\frac{7}{64}\frac{\gamma_{\text{dry}}^2}{\gamma_{\text{sat}}^2}\left(1+\frac{15}{7}\frac{\gamma_{\text{dry}}^4}{\gamma_{\text{sat}}^4}\right),\\
W_{\Delta_{14}} &= \frac{\gamma_{\text{dry}}^2}{32\gamma_{\text{sat}}^2}\left(1+5\sin^2\theta\right)-\frac{\gamma_{\text{dry}}^4}{64\gamma_{\text{sat}}^4}\sec^2\theta-\frac{1}{64}\left(1+9\sin^2\theta\right),\\
W_{\Delta_{15}} &= \left(\frac{\gamma_{\text{dry}}^2}{4\gamma_{\text{sat}}^4}-\frac{1}{2\gamma_{\text{sat}}^3}\right)\left(1-\frac{\gamma_{\text{dry}}^2}{\gamma_{\text{sat}}^2}\right)\sin^2\theta-\frac{15}{64}\frac{\gamma_{\text{dry}}^6}{\gamma_{\text{sat}}^6}\left(1-\frac{3}{15}\sin^2\theta\right)\\
&\quad +\frac{23}{64}\frac{\gamma_{\text{dry}}^4}{\gamma_{\text{sat}}^4}\left(1-\frac{3}{23}\sin^2\theta\right)-\frac{\gamma_{\text{dry}}^2}{8\gamma_{\text{sat}}^2},\\
W_{\Delta_{16}} &= \frac{3}{4\gamma_{\text{sat}}^2}\left(1-\frac{1}{\gamma_{\text{sat}}}\right)\sin^2\theta-\frac{\gamma_{\text{dry}}^2}{8\gamma_{\text{sat}}^2}\left(1-\frac{2}{\gamma_{\text{sat}}^2}\right)\sin^2\theta-\frac{\gamma_{\text{dry}}^4}{64\gamma_{\text{sat}}^4}\sec^2\theta,\\
W_{\Delta_{17}} &= \left(1-\frac{\gamma_{\text{dry}}^2}{\gamma_{\text{sat}}^2}\right)\left(\frac{9}{64}\sin^2\theta-\frac{1}{8\gamma_{\text{sat}}}\sin^2\theta-\frac{1}{64}\right),\\
W_{\Delta_{18}} &= -\frac{\gamma_{\text{dry}}^2}{64\gamma_{\text{sat}}^2}\left(1-9\sin^2\theta\right)-\frac{1}{16\gamma_{\text{sat}}}\left(1+2\frac{\gamma_{\text{dry}}^2}{\gamma_{\text{sat}}^2}\right)\sin^2\theta-\frac{1}{8\gamma_{\text{sat}}^2}\sin^2\theta,\\
W_{\Delta_{19}} &= \left(1-\frac{\gamma_{\text{dry}}^2}{\gamma_{\text{sat}}^2}\right)\left(\frac{\sin^2\theta}{4\gamma_{\text{sat}}^2}-\frac{\gamma_{\text{dry}}^2}{32\gamma_{\text{sat}}^2}\sec^2\theta\right).
\end{aligned}
$$

For clarification on how to derive the first order poroelastic approximation, let us re-look at Keys (1989) equation as it is described from the original report. It takes the form of

$$\begin{bmatrix} -X & -\sqrt{1-B^2X^2} & CX & -\sqrt{1-D^2X^2} \\ \sqrt{1-X^2} & -BX & \sqrt{1-C^2X^2} & DX \\ 2B^2X^2\sqrt{1-X^2} & B(1-2B^2X^2) & 2AD^2X\sqrt{1-C^2X^2} & -AD(1-2D^2X^2) \\ -(1-2B^2X^2) & 2B^2X\sqrt{1-B^2X^2} & AC(1-2D^2X^2) & 2AD^2X\sqrt{1-D^2X^2} \end{bmatrix} \times \begin{bmatrix} R_{\text{PP}} \\ R_{\text{PS}} \\ T_{\text{PP}} \\ T_{\text{PS}} \end{bmatrix} = \begin{bmatrix} X \\ \sqrt{1-X^2} \\ 2B^2X\sqrt{1-X^2} \\ 1-2B^2X^2 \end{bmatrix}, \tag{A4}$$

where

$$A = \frac{\rho_1}{\rho_0}, B = \frac{V_{S_0}}{V_{P_0}}, C = \frac{V_{P_1}}{V_{P_0}}, D = \frac{V_{S_1}}{V_{P_0}}, X = \sin\theta \tag{A5}$$

and R_{PP}, R_{PS}, T_{PP}, and T_{PS} are the possible reflections and transmissions of an incoming P-wave. As explained in equations (12) - (14), we can re-express the ratios in (A5) so that equation (A4) can be analyzed for fluid, shear, and density fluctuations instead of P-wave speed, S-wave speed, and density changes. Once these substitutions are made, we can place them back into (A4). The next step is the truncation step and it is the same procedure that is performed on each element of Keys (1989) equation. We will use the 4-4 entry of equation (A4) and demonstrate the process. In terms of poroelastic constants, this entry will be

$$A_{44} = \frac{2}{\gamma_{\text{sat}}^2}(1-a_\mu)^{-1}(\sin\theta)\sqrt{1-\frac{(1-a_\mu)^{-1}(1-a_\rho)}{\gamma_{\text{sat}}^2}\sin^2\theta} \tag{A6}$$

where $\gamma_{\text{sat}} = V_{P_0}/V_{S_0}$. We will then approximate this equation by using the Taylor series for $(1-a_\mu)^{-1} = 1 + a_\mu + a_\mu^2 + ...$ and the terms under the square root will be expanded around $\sin^2\theta$ where $(1-c\sin^2\theta)^{1/2} = 1 - \frac{1}{2}c\sin^2\theta - \frac{1}{8}c^2\sin^4\theta - ....$ Replacing these Taylor series into (A6) will yield

$$\begin{aligned} A_{44} = \frac{2}{\gamma_{\text{sat}}^2}[1+a_\mu+a_\mu^2+...](\sin\theta)\Bigg(1 - \frac{1}{2}\frac{[1+a_\mu+a_\mu^2+...](1-a_\rho)}{\gamma_{\text{sat}}^2}\sin^2\theta \\ -\frac{1}{8}\frac{[1+a_\mu+a_\mu^2+...]^2(1-a_\rho)^2}{\gamma_{\text{sat}}^4}\sin^4\theta - ...\Bigg). \end{aligned} \tag{A7}$$

After completing the necessary substitutions and expansions into the other elements of the 4x4 matrix, we can then use Cramer's rule to explicitly define an expression for R_{PP} which will theoretically contain all orders of perturbation models. Using Cramer's rule, in our purposes, is defined as

$$R_{\text{PP}} = \frac{\det \mathbf{P}_P}{\det \mathbf{P}}. \tag{A8}$$

where $\mathbf{P}_P$ is the augmented matrix in equation (A4) which means that its first column entries are replaced by the column vector from the right hand side and $\mathbf{P}$ simply represents the

original matrix before the replacement. Innanen (2011a) demonstrates this by expressing $R_{\rm PP}$ in terms of groupings of like-ordered model parameters and provides a more rigorous explanation of this process. After this step, we can then decide which terms to truncate from equation (A8) and that will determine the level of precision that is desired.

REFERENCES

Aki, K., and Richards, P. G., 2002, Quantitative seismology, 2nd ed.

Biot, M. A., 1941, General theory of three-dimensional consolidation: Journal of Applied Physics, **12**.

Castagna, J. P., Swan, H. W., and Foster, D. J., 1998, Framework for AVO gradient and intercept interpretation: Geohpysics, **63**.

Fatti, J. L., Smith, G. C., Vail, P. J., Strauss, P. J., and Levitt, P. R., 1994, Detection of gas in sandstone reservoirs using AVO analysis: A 3-D seismic case history using the Geostack technique: Geophysics, **59**.

Gassmann, F., 1951, Über die elastizitat poroser median: Vierteljahrsschrift der naturforschenden gesellschaft, **96**.

Gray, D., Goodway, B., and Chen, T., 1999, Bridging the Gap: Using AVO to detect changes in fundamental elastic constants: 69th Annual International Meeting, 852–855.

Innanen, K., 2011a, AVO analysis of P-, S-, and C-wave elastic and anelastic reflection data: CREWES Annual Report, **23**.

Innanen, K., 2011b, Hidden nonlinearities in the Aki-Richards approximation: CREWES Annual Report, **23**.

Innanen, K., 2011c, Matrix forms for the Knott-Zoeppritz equations: CREWES Annual Report, **23**.

Keys, R. G., 1989, Polarity reversals in reflections from layered media: Geophysics, **54**, 900–905.

Ostrander, W., 1984, Plane-wave reflection coefficients for gas sands at nonnormal angles of incidence: Geophysics, **49**, 1637–1648.

Russell, B. H., Gray, D., and Hampson, D. P., 2011, Linearized AVO and poroelasticity: Geophysics, **76**, C19–C29.

Russell, B. H., Hedlin, K., Hilterman, F. J., and Lines, L. R., 2003, Fluid-property discrimination with AVO: A Biot-Gassmann perspective: Geophysics, **68**, 29–39.

Shuey, R., 1985, A simplification of the Zoeppritz equations: Geophysics, **50**, 609–614.

Smith, G., and Gidlow, P., 1987, Weighted stacking for rock property estimation and detection of gas: Geophysical Prospecting, **35**, 993–1014.